INL/CON-22-67079-Revision-0

Evaluation and Comparison of a New Robust Waveform Against Direct Sequence Spread Spectrum for HF

August 2022

Brandon Hunt, Behrouz Farhang-Boroujeny, Thomas Cameron Sego, Hussein Moradi, Tom Holschuh, David Bryan Haab

Changing the World's Energy Future

INL is a U.S. Department of Energy National Laboratory operated by Battelle Energy Alliance, LLC

DISCLAIMER

This information was prepared as an account of work sponsored by an agency of the U.S. Government. Neither the U.S. Government nor any agency thereof, nor any of their employees, makes any warranty, expressed or implied, or assumes any legal liability or responsibility for the accuracy, completeness, or usefulness, of any information, apparatus, product, or process disclosed, or represents that its use would not infringe privately owned rights. References herein to any specific commercial product, process, or service by trade name, trade mark, manufacturer, or otherwise, does not necessarily constitute or imply its endorsement, recommendation, or favoring by the U.S. Government or any agency thereof. The views and opinions of authors expressed herein do not necessarily state or reflect those of the U.S. Government or any agency thereof.

INL/CON-22-67079-Revision-0

Evaluation and Comparison of a New Robust Waveform Against Direct Sequence Spread Spectrum for HF

Brandon Hunt, Behrouz Farhang-Boroujeny, Thomas Cameron Sego, Hussein Moradi, Tom Holschuh, David Bryan Haab

August 2022

Idaho National Laboratory
Idaho Falls, Idaho 83415

http://www.inl.gov

Prepared for the
U.S. Department of Energy
Under DOE Idaho Operations Office
Contract DE-AC07-05ID14517

Evaluation and Comparison of a New Robust Waveform Against Direct Sequence Spread Spectrum for HF

Brandon T. Hunt[1], David B. Haab[1], Thomas Cameron Sego[2], Tom V. Holschuh[2], Hussein Moradi[2], and Behrouz Farhang-Boroujeny[1]

[1]University of Utah; brandon.t.hunt@utah.edu, david.haab@utah.edu, farhang@ece.utah.edu
[2]Idaho National Laboratory; thomas.sego@inl.gov, tom.holschuh@inl.gov, hussein.moradi@inl.gov

Summary

This paper provides a comprehensive performance comparison between a filter bank multicarrier spread-spectrum (FBMC-SS) waveform and a current robust military waveform; namely, MIL-STD-188-110D, Waveform 0, proposed for communications through ionospheric/skywave HF channels. Waveform 0 is effectively a direct sequence spread spectrum waveform that uses the Walsh multi-codes to enhance its information transmission rate. It may thus be referred to as Walsh-DSSS. FBMC-SS, on the other hand, makes use of filter banks to hold its excellent performance, even when the received signal is subject to partial band interference. Successful application of FBMC-SS for communications across skywave HF channels has been previously demonstrated both theoretically and through experimental work. However, very little has been done to contrast FBMC-SS against Walsh-DSSS. The goal of this paper is to examine the performance of the FBMC-SS waveform against Walsh-DSSS when both are applied for communications across skywave HF channels. The two waveforms are compared both through a theoretical study and through experimental works across several skywave channels ranging from hundreds to thousands of kilometers.

1 Introduction

Classical high frequency (HF) skywave channels, spanning from 3 MHz to 30 MHz, offer long link-distances relative to other frequency bands. In the early days of radios, these long links were widely used for radio broadcasting. Recently, this part of the spectrum is used by military for establishing radio links in certain scenarios where cellular networks may not be available and satellite communications may be infeasible due to cost or atmospheric conditions [1–3]. Communications among vehicles at the sea that are spread across hundreds or thousands of miles is

This manuscript has been authored by Battelle Energy Alliance, LLC under Contract No. DE-AC07-05ID14517 with the U.S. Department of Energy. The United States Government retains and the publisher, by accepting the article for publication, acknowledges that the United States Government retains a nonexclusive, paid-up, irrevocable, world-wide license to publish or reproduce the published form of this manuscript, or allow others to do so, for United States Government purposes. STI Number: INL/CON-22-67079

a particular case of interest as the HF domain offers an alternative to satellite communications for over-the-horizon links [4, 5]. Additionally, compact and versatile wideband HF antenna designs have been developed which facilitate the deployment of HF transceivers over these mobile stations [6].

Beyond military use, the unique features of the HF band may be of interest to first responders, particularly in disaster situations where cellular networks may collapse due to various factors, such as overloading [7]. HF links also provide low-latency connections that can outperform some fiber-optic links while allowing the transmitter and receiver to remain dynamic in space [8]. Both military applications and first responders' needs have fueled interest in developing new HF transmission techniques that are more robust than the established methods.

A common approach for developing robust waveforms is to spread the signal energy across time, creating redundancy in the signal. This approach results in a direct-sequence spread-spectrum (DSSS) waveform [9], granting the receiver the ability to distinguish multipath components and resolve inter-symbol interference in frequency-selective channels [10]. This spreading allows DSSS to achieve a given bit error rate at 10 dB or less SNR than waveforms that do not make use of spread-spectrum techniques, [11].

The U.S. Military standard, MIL-STD-188-110D, Appendix D, [1], lists fourteen waveforms for use in HF links that support various data rates over different bandwidths. Among these, waveform number 0, in particular, is designed to perform robustly in the harshest scenarios encountered in HF links. This waveform is a special form of DSSS that makes use of multiple Walsh codes and different bandwidths to establish various data rates. It can support data rates from 75 to 1200 bits/s over bandwidths of 3 to 48 kHz. In this paper, we refer to this waveform as both Walsh-DSSS and, simply, Walsh.

A more recent robust waveform that has been developed by our research group is termed filter bank multicarrier spread spectrum (FBMC-SS), [12–17]. As its name implies, this waveform makes use of a filter bank to develop a spread spectrum technique. The spread spectrum chips are spread across a number of subcarrier bands instead of across time as is done in DSSS. One unique feature of FBMC-SS is that it can easily mask portions of the band that are corrupted by high-power interferers [17, 18].

Resistance to interference is critical for waveforms used in the HF regime. Because the HF domain offers link distances, the spectrum can become polluted with narrowband interferers from around the globe [3, 4, 11]. The issue of interference is compounded by the poor out-of-band suppression of transmitters often used for HF communications [19]. Hence, the ability of FBMC-SS to easily filter interference lends itself well for use in the HF band.

As of today, most of the studies of FBMC-SS in the domain of HF communications have been limited to its fine-tuning without much attention to its performance relative to more established waveforms, though some limited study can be found in [20].

Waveform performances are compared through both simulated and over-the-air (OTA) testing. OTA results have been gathered over short-range, medium-range, and long-range channels to validate the conclusions drawn in this paper with a substantial amount of data.

Parts of the results presented in this paper have been previously disseminated in [22] and [23]. In [22], only the first method of multicode scrambling of Section III-D here has been presented. In [23], the second multicode technique has been presented. Further, some simulation results presented in this paper have been given in [22,23]. Although these results have been presented in previous works, we provide them again here as these simulation results are necessary to establish the fundamental performance characteristics of the two waveforms. In this work, the simulated results are summarized and OTA results from a long-haul, latitudinal HF link are given.

The rest of this paper is organized as follows. The relevant details of the Walsh waveform

are summarized in Section 2. A brief overview of the transceiver system for the FBMC-SS is presented in Section 3. The system parameters used in the testing as well as explicit definitions of bandwidth and SNR are given in Section 4. The simulation results are presented in Section 5, and the experimental results are discussed in Section 6. Concluding remarks are made in Section 7.

2 Walsh-DSSS Waveform

As mentioned above, the Walsh waveform of MIL-STD-188-110D, Appendix D [1] is a unique form of DSSS in which the spreading vectors that define the data symbols are a set of Walsh codes; i.e., the columns of a Walsh matrix. At the transmitter, to generate the output waveform, the input bit sequence is arranged into bit-groups that are then mapped to Walsh-encoded orthogonal BPSK chip sequences. Following [1], the length of these chip sequences depends on the signal bandwidth. Specifically, signals with nominal bandwidths of 18 kHz or lower encode groups of 2 bits with 32-length chip sequences, whereas nominal bandwidths between 21 kHz to 48 kHz spread groups of 4 bits to 64-length sequences. Accordingly, the diversity gain achieved by Walsh-DSSS is equal to the length of the chip sequence [9]. Each 32-length chip sequence is formed by repeating a Walsh code of length 4, eight times. On the other hand, each 64-length chip sequence is formed by repeating a Walsh code of length 16, four times.

The Walsh-encoded BPSK chip sequence is subsequently modulated by an 8-PSK scrambling code which serves to whiten the spectrum of the signal in the frequency domain and reduce ISI in the time domain, [1, 4]. Without this scrambling sequence, the signal appears in the frequency domain as a number of tones due to the repetition of the Walsh codes. Consequently, if a deep channel fade were to align with one of these tones, considerable signal energy would be lost. By scrambling the transmit sequence, the signal energy is spread evenly over the transmission band thereby reducing the impact of severe channel fades. This scrambling also has the benefit of making successive Walsh symbols quasi-orthogonal, reducing the ISI that may be introduced by multipath in the channel.

At the receiver, the scrambling sequence is undone, returning the scrambled 8-PSK sequence to the original, orthogonal BPSK Walsh codes. A RAKE is then used to recombine signal energy from any multipath fading present in the channel. A channel estimate for the RAKE is initially generated by averaging together a number of channel estimates obtained from individual periods of the pilot sequence. From this initial estimate, a decision-directed channel update algorithm may be employed to track variations in the channel, [24]. Unfortunately, our simulations as well as OTA experiments have shown that this method may not always work as decision errors can lead to an incorrect adaptation of the receiver.

3 FBMC-SS Waveform

The multicarrier system presented in this paper is based on a filter bank multicarrier spread spectrum (FBMC-SS) waveform developed in [12, 25–27] and further explored in [14, 16, 18]. This waveform uses multiple, non-overlapping adjacent subcarriers to carry data symbols. With this waveform, spreading is performed across all of its subcarriers and not across time. In [14], FBMC-SS is shown to be well suited for HF communications because of its robustness and low-PAPR.

The processing gain is accordingly controlled by the number of subcarriers. In a typical design of FBMC-SS, each subcarrier increases the processing gain of the waveform by 2 [16];

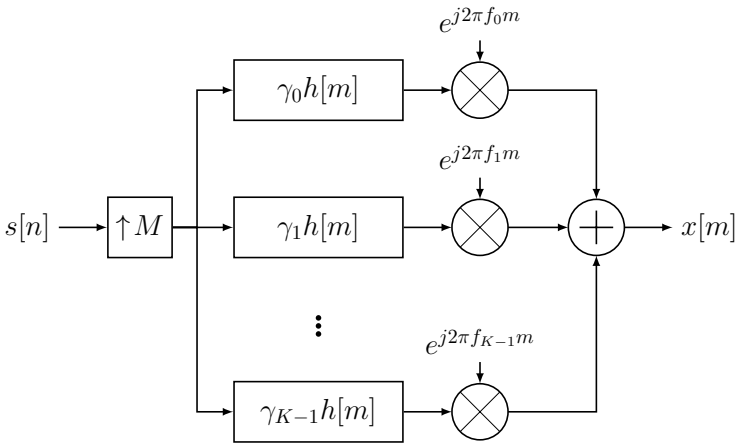

Figure 1: FBMC-SS Transmitter Structure

hence, for a waveform with K subcarriers, we achieve a processing gain

$$\mathcal{G} = 2K. \tag{1}$$

3.1 Transmitter

A block diagram of the FBMC-SS transmitter is given in Fig. 1. Here, the data symbol sequence $s[n]$ is upsampled by a factor of M. This upsampled signal is split amongst K parallel branches and the k-th branch is multiplied by a spreading gain γ_k. It is assumed that

$$|\gamma_k| = 1, \quad \text{for } k = 0, 1, \ldots, K-1, \tag{2}$$

such that each γ_k acts as a rotation in the complex plane. Each rotated symbol copy is then independently filtered by a square-root raised-cosine pulse-shaping filter $h[m]$ with an excess bandwidth of 100% and modulated to the respective subcarrier band. The analog center frequency of the k-th subcarrier is denoted by F_k. To ensure the subcarriers do not overlap, the subcarrier frequencies should be selected according to

$$F_k = \frac{K - (2k+1)}{T_b}, \quad \text{for } k = 0, 1, \ldots, K-1, \tag{3}$$

where T_b is the symbol interval. The corresponding digital frequency f_k (with units of cycles/sample) is found as

$$f_k = F_k T_s, \tag{4}$$

where T_s is the sampling interval. Note that the index n refers to the symbol index whereas m refers to the sample index which operates at a rate M times faster, where $M = 2K$ to preserve the relationship given in eqn. (1) [16]. The transmit signal can thus be expressed as

$$x[m] = \sum_{n} \sum_{k=0}^{K-1} s[n] \gamma_k h\left[m - nM\right] e^{j2\pi f_k m}. \tag{5}$$

The branches of the transmitter may be collapsed into a single filter, $g[m]$, given by

$$g[m] = \sum_{k=0}^{K-1} \gamma_k h[m] e^{j2\pi f_k m}, \tag{6}$$

leading the following simplification of (5),

$$x[m] = \sum_{n} s[n]g[m - nM]. \tag{7}$$

Clearly, here, $x[m]$ is at baseband. It should be modulated to an RF band before transmission and, at the receiver, the corresponding demodulation should be applied before proceeding with the steps that are discussed next.

3.2 Receiver

In a conventional implementation, the received signal (after demodulation) is first passed through an analysis filter bank (AFB) for separation of the content of different subcarrier bands. The results of this analysis are then recombined through a maximum ratio combiner that aims to maximize the signal to noise plus interference ratio at the output. This receiver structure is called the AFB-based receiver in [17].

An alternative receiver structure makes use of a matched filter with power normalization at different subcarrier bands. This structure has been recently developed and presented in [17], and is termed NMF-based receiver, where NMF stands for normalized matched filter. This structure is used throughout this paper as opposed to the AFB design used in previous works. For detailed comparisons of the AFB- and NMF-based receiver performances, an interested reader may refer to [17]. An important point to note about the NMF is that the normalization operation becomes sub-optimal at higher SNRs which, under typical use cases, is not problematic as this waveform primarily operates at negative SNRs.

Unlike the Walsh-DSSS, the FBMC-SS system does not require a decision-directed channel tracking algorithm because known pilot symbols are inserted every 8 data symbols for the purposes of tracking the channel. We note that while the inserted pilots incur some overhead, they offer the advantage of deploying effective and reliable channel tracking.

3.3 Multicodes

Similar to Walsh-DSSS, to increase the spectral efficiency and data-rate of FBMC-SS, a method of applying multicodes should be adopted. A method of generating and using multicodes for use with FBMC-SS that maintains its low-PAPR is presented in [13], and is briefly repeated here. This method begins by redefining the spreading gain vector as

$$\mathbf{a}_0 = \frac{1}{\sqrt{K}} \begin{bmatrix} \gamma_0 \\ \gamma_1 \\ \vdots \\ \gamma_{K-1} \end{bmatrix}. \tag{8}$$

Here, the addition of the factor $\frac{1}{\sqrt{K}}$ on the right-hand side of (8) is to normalize the vector $\mathbf{a}_0$ to a magnitude of 1; recall that $|\gamma_k| = 1$, for $k = 0, 1, \cdots, K-1$. Starting with $\mathbf{a}_0$, we construct the following basis set

$$\mathbf{a}_i = \frac{1}{\sqrt{K}} \begin{bmatrix} \gamma_0 e^{j\frac{2\pi i}{K}\times 0} \\ \gamma_1 e^{j\frac{2\pi i}{K}\times 1} \\ \vdots \\ \gamma_{K-1} e^{j\frac{2\pi i}{K}\times (K-1)} \end{bmatrix}, \quad 0 \le i \le K-1. \tag{9}$$

It is straightforward to show that the basis vectors $\mathbf{a}_i$, for $i = 0, 1, \cdots, K-1$, constitute an orthogonal set. Hence, they may be used to represent blocks of $\log_2 K$ coded bits by modulating the spreading gain of each subcarrier. This encoding method can be applied in addition to the data encoding on the input symbol sequence $s[n]$ from Fig. 1, hence the name multicode. However, mirroring the approach taken by Walsh-DSSS in [1], $s[n]$ may also be set equal to one for all values of n such that the transmitted information is coded entirely by the multicodes. Here, to remain consistent with Walsh-DSSS, the latter method is adopted.

3.4 Scrambling

As noted earlier in Section 2, Walsh-DSSS modulates the generated BPSK spread spectrum signal by an 8-PSK scrambling sequence to decorrelate the synthesized data symbols, reducing the impact of ISI across the transmitted information. In FBMC-SS, scrambling has to be formulated in such a way that it has no adverse effects on the PAPR of the resulting signal. Here, we discuss two methods of suppressing ISI via multicode scrambling while preserving the low PAPR and have equivalent ISI impacts to the scrambling method used by Walsh-DSSS.

The first method makes use of the fact that, typically, the number of multicodes used for a specific case is a subset of the entire set of available multicodes. For instance, in Walsh-DSSS with nominal bandwidths less than 18 kHz, the 32-length chip sequences are drawn from a set of 32 multicodes. However, only a subset of size 4 of these multicodes are used for data mapping.

For FBMC-SS, we propose that one may cycle through the unused subsets of the multicodes over successive data symbols. For the case where a Walsh waveform uses 32-length spreading sequences to encode $B = 2$ bits/sym., a corresponding FBMC-SS system with equal processing gain will have $K = 16$ subcarriers (via eqn. (1)). Hence, the full set contains 16 multicodes, but we need to choose only $2^B = 4$ of them. Therefore, there are also 4 disjoint subsets of orthogonal symbol vectors that may be cycled through with respect to symbol time. This setup can be robust to multipaths and ISIs that span up to four multicode symbol intervals.

This method, while straightforward to implement, is restrictive as it limits the maximum bitrate for an orthogonal symbol set to be $B \leq \lfloor \log_2 K - 1 \rfloor$ bits/sym. Hence, in cases where the bit rate may need to be maximized, the following scrambling method is preferred.

We recall from [14] that the choices of the spreading gain parameters γ_k which result in a reasonably low PAPR can be made by using the Friese algorithm of [28]. The Friese algorithm is designed to minimize the PAPR of any summation of tones in the form of

$$\rho[m] = \sum_k \gamma_k e^{j2\pi f_k m}. \tag{10}$$

In [14], it is shown that the pulse shaping filter $g[m]$ may be factored as

$$g[m] = h[m]\rho[m]. \tag{11}$$

It is then argued that since $h[m]$ is a smooth pulse with no significant peak, any peak in $g[m]$ that may lead to a significant increase in the PAPR of the synthesized signal $x[m]$ can only be brought in by peaks in $\rho[m]$. Hence, minimizing the PAPR of $\rho[m]$ will result in a synthesized FBMC-SS signal $x[m]$ with a low PAPR.

Another observation which may be made is that there exist many solutions to the set of the spreading gains γ_k that lead to a low PAPR as the solution-space contains many local minima. Such solutions can be found by randomly initializing the parameters γ_k and running the Friese algorithm a number of times. In [23], it was found that low-PAPR spreading gain solutions have

similar statistical properties to randomly-generate spreading gains; i.e., the solutions are largely uncorrelated.

Therefore, since each vector of spreading gains has a large probability of being near-orthogonal with another constituent in the set, the spreading gains can be used to de-correlate the data symbols in time. For every transmitted symbol, a pre-determined spreading gain vector will be applied at the transmitter to "scramble" the data symbol, and the same vector used at the receiver to "unscramble" the symbol. This operation is similar to how the Walsh waveform applies a pseudo-random 8-PSK scrambling sequence; here, we also scramble each symbol using a set of random phases. The key difference is that here, because we are using a multicarrier waveform, each subcarrier uses a different scrambling sequence.

It may be noted that this second scrambling method results in a more complex structure when the NMF-based receiver is adopted. In this case, a set of parallel NMFs must be implemented—one for each spreading gain vector. This may increase the receiver complexity significantly. On the other hand, when an AFB-based receiver is deployed, there will be no significant change in the receiver complexity.

4 Test Parameters

As mentioned in Section 2, there are numerous bandwidths of the Walsh waveform specified in [1]. This paper focuses on the 18 kHz and 48 kHz nominal bandwidths which possess processing gains of 32 and 64, respectively.

To make a valid comparison, a corresponding FBMC-SS system may be configured in two ways: either the processing gains or the bandwidths of the FBMC-SS systems may be matched to the associated Walsh waveforms. In this paper, we proceed in both ways.

First, we develop waveforms with equal processing gain. The 18 kHz Walsh waveform has a coded bitrate of 900 bits/sec, 2 bits are encoded by each Walsh sequence, it has a null-to-null bandwidth of 19.4 kHz, and a processing gain of 32. Recalling that the processing gain of an FBMC-SS waveform is $\mathcal{G} = 2K$, a corresponding FBMC-SS waveform with equal processing-gain will have 16 subcarriers. To match the modulation order, each FBMC-SS symbol should encode 2 bits. Hence, the symbol rate of the FBMC-SS waveform will be 450 sym/sec, and with the prototype filters having an excess bandwidth of 100%, each subcarrier will have a null-to-null bandwidth of 900 Hz. The bandwidth of the resulting waveform is accordingly $16 \times 900 = 14.4$ kHz.

Exchanging the order of steps taken, we can derive another waveform that is instead matched to the bandwidth of the Walsh waveform. The data rate and symbol rate of this FBMC-SS waveform will remain the same as above; hence, the subcarriers will have the same bandwidth of 900 Hz. Therefore, the associated FBMC-SS waveform should have 19.4 kHz$/900$ Hz $= 21.6$ subcarriers. Rounding down (so that the Walsh bandwidth remains greater than that of the FBMC-SS) to the nearest even number results in a waveform with 20 subcarriers and a bandwidth of 18 kHz. Note that in this scenario, the processing gain is 40, exceeding that of the associated Walsh waveform.

Similar steps may be taken to derive the FBMC-SS waveforms matched to the 48 kHz Walsh waveform. A summary of the waveform parameters is presented in Table 1. Throughout this document, the first three waveforms (1w, 1a, 1b) listed in Table 1 will be referred to as the group 1 waveforms and the last three waveforms (2w, 2a, 2b) will be referred to as the group 2 waveforms.

Note that the bandwidths of the Walsh waveforms specified in Table 1 are larger than the nominal values of 18 and 48 kHz given in [1]; this is due to the pulse-shaping filter, which

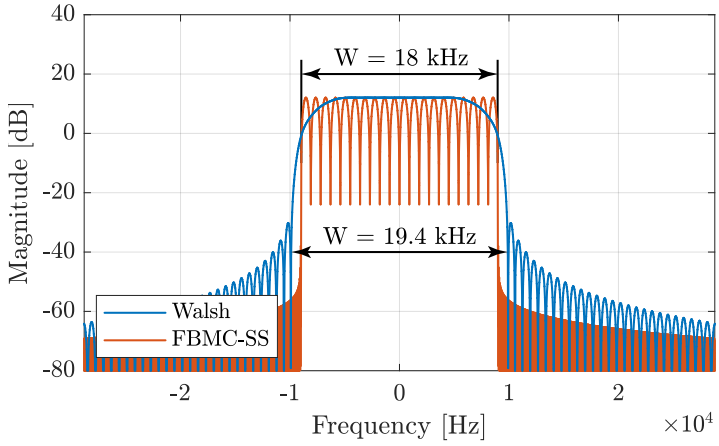

Figure 2: Spectra of transmitted Walsh-DSSS and FBMC-SS waveforms

has an excess bandwidth of 35%. To make this point clear, Fig. 2 presents the spectra of the Walsh and 20 subcarrier FBMC-SS waveforms for the case of an 18 kHz nominal bandwidth. From these spectra, it appears that the bandwidth listed in MIL-STD-188-110D for the Walsh waveform is considered as the portion of its spectrum which is within 10 dB of its flat top.

Both the simulated results of Section 5 and the OTA results of Section 6 use packets containing 1024 bits for a toal duration between 0.5 and 1 seconds for groups 1 and 2 waveforms, respectively. Additionally, here, no FEC is used; hence, the presented BER curves are those of uncoded information.

4.1 Signal-to-Noise Ratio

A key parameter used while characterizing the systems' performances is the signal-to-noise ratio (SNR). Here, SNR is defined as the power of the received signal divided by the power of the noise over the signal bandwidth at the receiver input. That is,

$$\text{SNR} = 10\log_{10}\Big(\frac{P_s}{N_0 W}\Big), \tag{12}$$

where P_s denotes the power of the signal at the receive antenna, N_0 is the noise spectral density in units of Watts/Hz, and W is the signal bandwidth. It is important to note that the noise energy is considered only over the bandwidth of the signal, and the bandwidth W includes the roll-off of the pulse-shaping filters—W is the null-to-null bandwidth of the signal.

The bandwidth of the Walsh waveform can be found as $W = \frac{F_d}{B} \times L_W(1+\alpha)$ Hz, where F_d is the data rate with units of bits/sec, B indicates the number of bits per Walsh symbol, L_W

Table 1: Tested waveform parameters

Waveform Number	Scheme	Bandwidth	Processing Gain
1w	Walsh	19.4 kHz	32
1a	FBMC-SS	14.4 kHz	32
1b	FBMC-SS	18 kHz	40
2w	Walsh	51.8 kHz	64
2a	FBMC-SS	38.4 kHz	64
2b	FBMC-SS	48 kHz	80

is the length (in chips) of each Walsh symbol, and α is the roll-off factor of the pulse-shaping filter; $\alpha = 0.35$ according to MIL-STD-188-110D, Appendix D. Similarly, the bandwidth of the FBMC-SS waveform is $W = \frac{F_d}{B} \times K(1+\alpha)$, where K is the number of subcarriers, and $\alpha = 1$ for FBMC-SS. For performance evaluations, bit-error rate (BER) versus SNR curves will be presented in the subsequent sections of this paper.

4.2 Pilot Overhead

As mentioned in Sections 2 and 3, both waveforms can track changes in the channel over the duration of the packet.

The Walsh uses a decision-directed method that assumes the decoded symbols are correct and generates corresponding channel estimates. This method requires no additional pilot symbols beyond the preamble section. However, to prevent error propagation, it is important to begin with an accurate, low-noise channel estimate. Consequently, a large number of pilot symbols are transmitted at the preamble of the Walsh waveform.

In contrast, the FBMC-SS waveform tracks channel changes via pilot symbols inserted every 8^{th} data symbol. In this case, fewer pilot sequences may be transmitted at the beginning of the packet because this method is not prone to error propagation.

For the results presented herein, we consider 24 periods of the pilot sequence for the Walsh waveforms. As detailed in MIL-STD-188-110D, Appendix D, for the 18 kHz and 48 kHz waveforms, a single period of the pilot sequence is either 192 chips or 256 chips in length, respectively. The resultant pilot sequences are thus 4608 and 6144 chips for the 18 and 48 kHz Walsh waveforms, respectively.

We define pilot overhead OH as the ratio of the duration of pilot symbols to the duration of the entire packet. That is,

$$\text{OH} = 100 \times \frac{T_{\text{pilot}}}{T_{\text{pilot}} + T_{\text{payload}}}. \tag{13}$$

Here, we find that for the 1w waveform using 24 periods of pilot sequences with a payload of 16384 chips, the pilot overhead is $\text{OH} = 21.9\%$. The associated FBMC-SS waveforms (1a and 1b), with pilots inserted every 8^{th} data symbol and a preamble of 64 symbols, have an overhead of $\text{OH} = 21.1\%$.

Similarly, for the 2w waveform, the pilot overhead for a payload with 16384 chips is $\text{OH} = 27.3\%$. The associated FBMC-SS waveforms (2a and 2b) again have pilots inserted every 8^{th} data symbol and contain 64 symbols in the preamble for an overhead of $\text{OH} = 28.3\%$.

The pilot overheads for both waveforms given here were adjusted to be roughly equal to maintain a fair comparison.

5 Simulated Results

Simulations are conducted to provide a benchmark for the OTA results. Three simulation environments are tested for each of the waveforms listed in Table 1: ideal (impulsive) channel conditions, simulated HF channel conditions, and HF conditions with interference. For each environment, results for the narrow bandwidth (group 1 waveforms listed in Table 1) and wide bandwidth (group 2 waveforms) are given. A summary of the simulation results are provided at the end in Section 5.4.

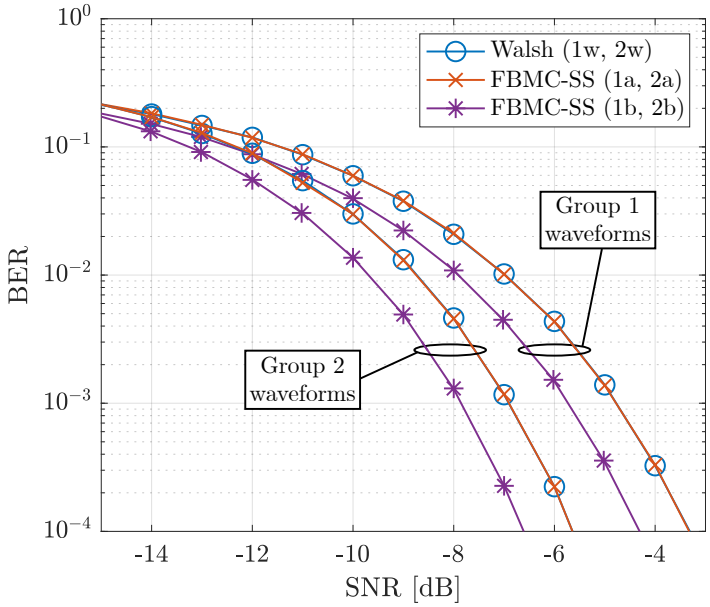

Figure 3: Ideal channel results comparing all 6 waveforms.

5.1 Ideal Channel Simulations

The first tests are conducted using an ideal (impulsive), AWGN channel with results presented in Fig. 3. Under these channel conditions, the system performance is primarily controlled by the processing gain. Hence, the 1w and 1a waveforms have the same performance, and the 1b waveform has superior performance due to its larger processing gain; a gain of $10\log_{10}(20/16) \approx 1$ dB is observed. Similar trends may be observed for the group 2 waveforms.

5.2 HF Channel Simulations

To provide more enlightening simulation results, waveform performances are next examined in three different simulated channel environments. The first environment is a time-invariant single-mode HF channel used to form a preliminary understanding of the impact the channel has against these waveforms. The second environment is a time-invariant 2-mode channel with equal-power modes. Lastly, the aforementioned one-mode channel is examined as a time-varying channel to observe any impairments introduced by the channel estimation and tracking techniques employed in both systems. For the first two channel environments, the receiver has perfect knowledge of the channel. For the third environment, the channel is estimated and tracked by the receivers. Results from the third channel environment are generated using the same receiver algorithms that will be used to process the OTA packets in the next section.

The HF channel that is used for our simulations is based off of the wideband HF model presented in [29]. This is in contrast to the traditionally used Watterson model [30]. The Watterson model is valid for traditional narrowband (3 kHz) waveforms because the RMS delay spread of HF channels is typically much smaller than the symbol intervals of these waveforms. However, this model becomes inaccurate when the symbol or chip interval of a waveform is on the order of or less than the delay spread which is true for the wideband waveforms presented herein. The model presented in [29] represents each channel mode by a number of taps, more closely emulating an actual HF channel at these bandwidths.

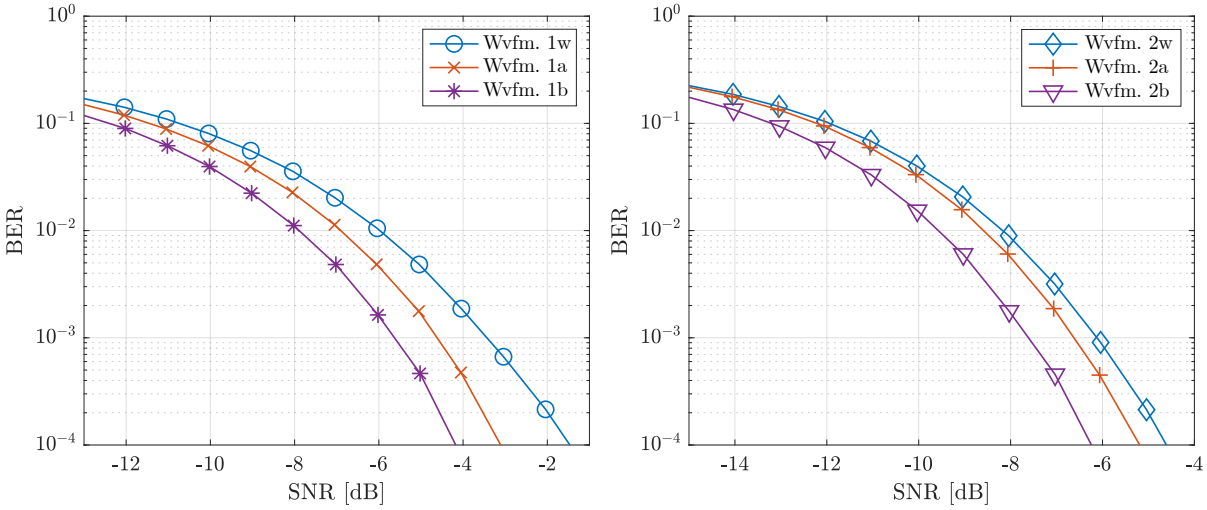

(a) Group 1 waveform performances.

(b) Group 2 waveform performances.

Figure 4: Simulated 1-mode HF channel results.

5.2.1 Single-mode channel

The simulated HF channel used for this section has a single mode with a delay spread of $T_d = 80$ μs which follows the "Daytime Quiet" channel model given in [14]. Additionally, the simulated channel is randomly generated for each packet, but is held constant for the duration of the packet; i.e., the channel is time-invariant. The results of this test are presented in Figs. 4a and 4b.

There is little difference here compared to the ideal-channel scenario because the simulated channel has a narrow delay spread relative to the symbol interval for the waveforms. The chip-interval of the Walsh-DSSS waveform is 69 μs for the 1w waveform and 26 μs for the 2w waveform. Thus, both Walsh-DSSS waveforms lose only a few chips to inter-chip interference. On the other hand, for the FBMC-SS system, the symbol intervals are 2.2 ms and 1.67 ms for the narrow (waveforms 1a & 1b) and wide (waveforms 2a & 2b) bandwidths, respectively. Hence, the channel acts as a single tap (within reasonable approximation) over each subcarrier band for the FBMC-SS system, so the performance is nearly identical to the ideal channel case.

5.2.2 Two-mode channel

To further examine the waveforms' performances, a two-mode time-invariant HF channel is used for simulation. The two modes are spaced by an amount equal to the symbol interval in order to observe maximum ISI. For the group 1 waveforms, the mode-spacing is $T_{\text{mode}} = T_b = 1/450$ sec; for the group 2 waveforms, $T_{\text{mode}} = T_b = 1/600$ sec. Note that because both systems employ methods to combat ISI (scrambling sequences in Walsh-DSSS, cyclic-symbol mapping in FBMC-SS), the performance loss in this case is expected to be minimal.

The results of these simulations are presented in Figs. 5a and 5b for the group 1 and group 2 waveforms, respectively. Note that compared to the 1-mode HF channel case, there is some additional loss; this is not due to ISI. Rather, this loss is due to signal energy lost from the destructive interference of the two modes.

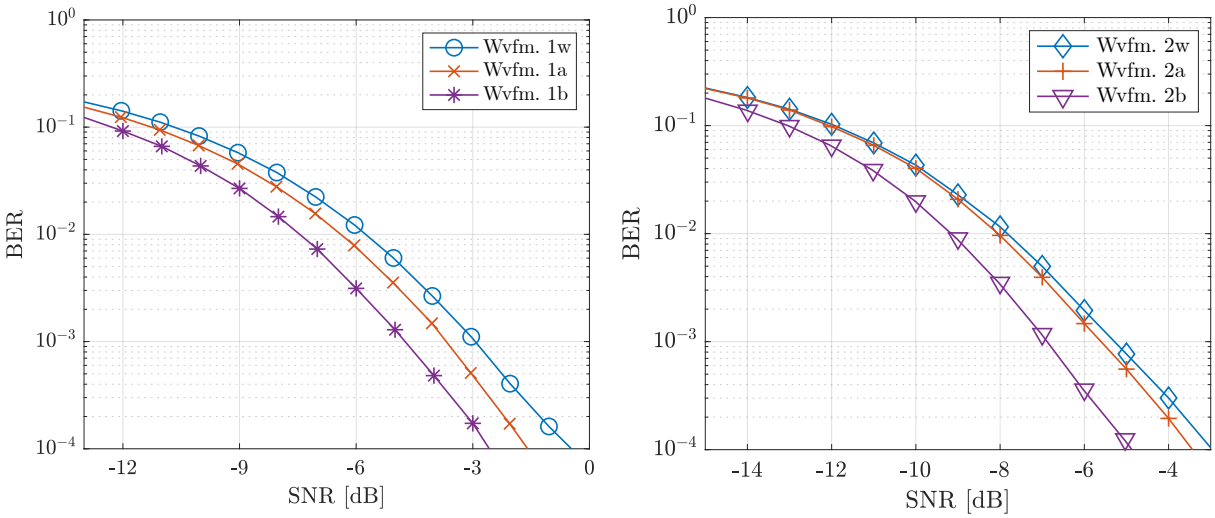

(a) Group 1 waveform performances.

(b) Group 2 waveform performances.

Figure 5: Simulated 2-mode HF channel results.

5.2.3 1-mode time-varying HF channel

The final simulation environment that is tested is a time-varying single-mode HF channel that most closely resembles HF skywave links. The channel has a doppler spread that follows the "Daytime quiet" channel model from [14]; that is, a Doppler spread of $D_s = 0.09$ Hz. Unlike the previous simulation environments, the receiver used in these tests does not have knowledge of the channel characteristics or timing information; i.e., the receiver is required to estimate all necessary parameters.

The results are given for waveforms 1w and 1a as an unconventional BER scatter plot in Fig. 6. In this figure, each dot represents a decoded packet. The dots have some vertical variation because the BER over each packet is based on a small number (1024) of transmitted bits. Here, the simulated BER curves which are obtained by averaging over a much larger number of bits are also presented for comparison. This style of BER plot is used extensively in Section 6 where the OTA results are presented.

The introduction of a time-varying channel results in the addition of inter-carrier interference (ICI) for the FBMC-SS system [31]. However, because the subcarrier filters are designed to have large stop-band attenuation as well as a wide transition band, performance loss due to ICI is minimal. Ultimately, the results from this test demonstrate that there is little performance loss between the receivers used in simulation and the receivers used for the OTA testing in Section 6; any error introduced by parameter estimation in the OTA receivers is minimal.

5.3 HF Channels with Interference

The waveform performances under the first two HF channel conditions from Section 5.2 are presented again here but with the addition of some constant interference.

For both cases, a 3 kHz wide interferer centered over the passband is added to the HF-channel signals. The interferer has a power spectral density 15 dB greater than the signal which is representative of interferer power levels typically seen in the HF domain. An example of observed HF interference is given in Fig. 7 which shows the spectrum of a received 40 subcarrier FBMC-SS waveform during OTA recording on September 15$^{\text{th}}$, 2021. In the presence of interference, the NMF-based structure of the FBMC-SS transceiver will weigh the affected subcarriers lower by

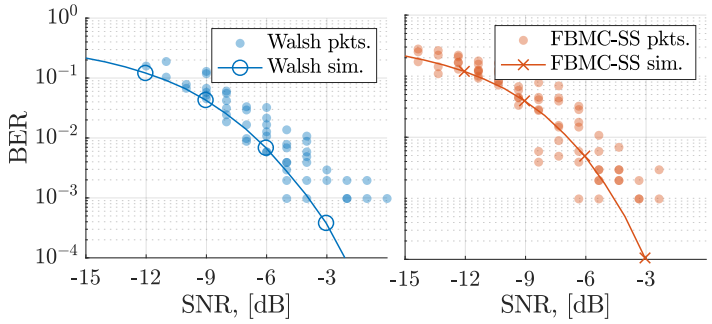

Figure 6: Simulated results of transmitting over a time-varying single-mode HF channel. The BER for a given packet is represented by a single point and the simulation result for the associated time-invariant channel is given for reference. *Left*: waveform 1w; *Right*: waveform 1b

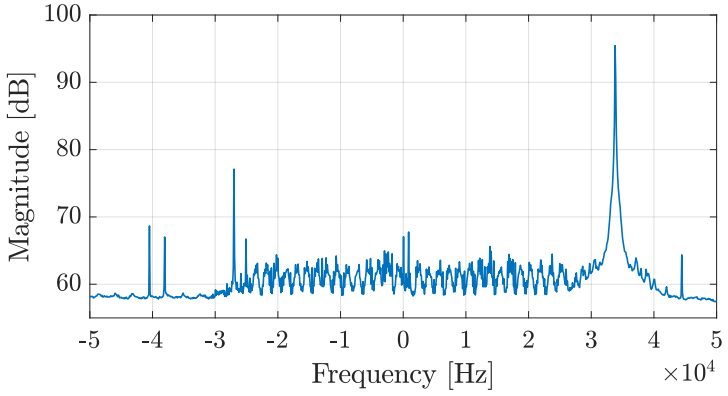

Figure 7: Spectrum of HF band (centered at 8.190 MHz) observed during OTA testing on March 13th. The subcarriers are clearly visible, and there is a large interferer roughly 35 dB greater than the signal centered around 33 kHz adjacent to our transmitted signal. Several narrowband interferers of lower power (10 to 20 dB greater than signal) occupy the spectrum over the passband as well. Note the FBMC-SS signal here is operating at positive SNR; this was done only for illustrative purposes.

virtue of the normalization step, [17]. The Walsh waveform, however, leverages only the spread-spectrum bandwidth widening to preserve the signal integrity and does not employ interference rejection techniques. Numerous interference suppression algorithms exist; but, they add significant complexity, [32, 33]. Hence, the results here demonstrate the intrinsic robustness of each waveform against narrowband interference without resorting to any advanced signal processing methods.

5.3.1 Single-mode time-invariant HF channel

The single mode channel presented here is the same channel used in Section 5.2.1. Results for this case are presented in Fig. 8a for the group 1 waveforms and in Fig. 8b for the group 2 waveforms.

The Walsh waveform incurs a substantial performance loss and, as SNR increases, approaches an unresolvable BER floor. For the 1w waveform, this is around a BER = 3.5×10^{-2}, which may not be reliably corrected by FEC. The 2w Walsh waveform has a floor near 2×10^{-3} which should be corrected by an FEC.

Similarly, the FBMC-SS waveform also incurs a performance loss; however, the loss does not result in a BER floor like the Walsh because the FBMC-SS waveform is able to weight the interfered subcarriers lower and recover the signal content in the unencumbered subcarriers. The

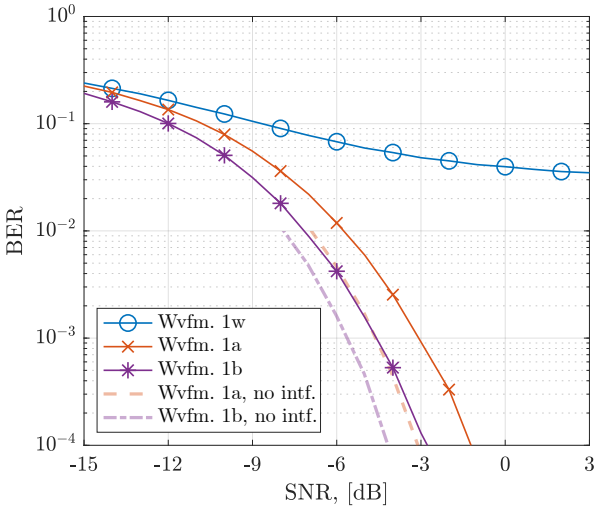

(a) Group 1 waveform performance. A loss of around 1 dB is observed for the 1b waveform, and a loss of around 1.5 dB for the 1a waveform.

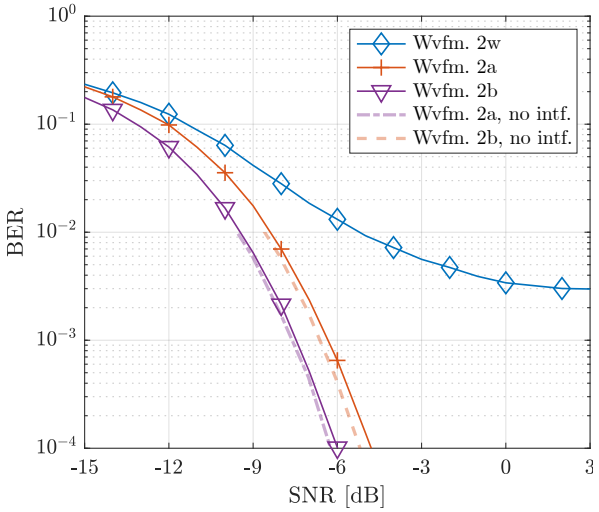

(b) Group 2 waveform performance. Both the 2a and 2b waveforms show minor performance degradation.

Figure 8: Simulated results of transmitting over a time-invariant 1-mode HF channel in the presence of a strong interferer. For the FBMC-SS systems, the non-interference results from Fig. 4 are presented again here as partial dashed lines for reference.

loss observed here is on the order of 1.2-1.8 dB for the group 1 FBMC-SS waveforms and is the result of two compounding factors.

First, the loss from the interference is expected to be comparable to the reduction of signal bandwidth. For the group 1 waveforms, each subcarrier has a bandwidth of 900 Hz, so the 3 kHz interference spans over 4 subcarriers, resulting in losses of $10\log_{10}(16/12) = 1.25$ dB and $10\log_{10}(20/16) = 0.97$ dB for the 16 and 20 subcarrier cases, respectively. Similarly for the group 2 waveforms whose subcarrier bandwidths are 1.2 kHz, the interference spans over 3 subcarriers, resulting in losses of 0.43 dB and 0.34 dB for the 32 and 40 subcarrier cases, respectively. Secondly, additional losses are incurred due to the fact that the NMF operation is merely an approximation of the maximum ratio combining (MRC) technique, [17]. For the system setups here, this sub-optimality manifests as a performance loss of between 0.2-0.5 dB for the group 1 waveforms and a negligible amount for the group 2 waveforms.

5.3.2 2-mode time-invariant HF channel

The 2 mode channel presented here is the same as used in Section 5.2.2. The results are presented in Figs. 9a and 9b for the group 1 and group 2 waveforms, respectively.

The performance in this case again follows the previous mode case. The loss due to the destructive interference resulting in lower received signal energy in this case is greater for the FBMC-SS than in the non-interfering case.

5.4 Summary of Simulated Results

The results presented in this section confirm several key properties of the NMF-based FBMC-SS receiver when contrasted against the Walsh. First, when the FBMC-SS waveform and the Walsh waveform are designed to have the same processing gain, the FBMC-SS waveform occupies less bandwidth than the Walsh. On the other hand, when the FBMC-SS and Walsh waveforms are designed to have the same bandwidth, the FBMC-SS waveform has a larger processing gain

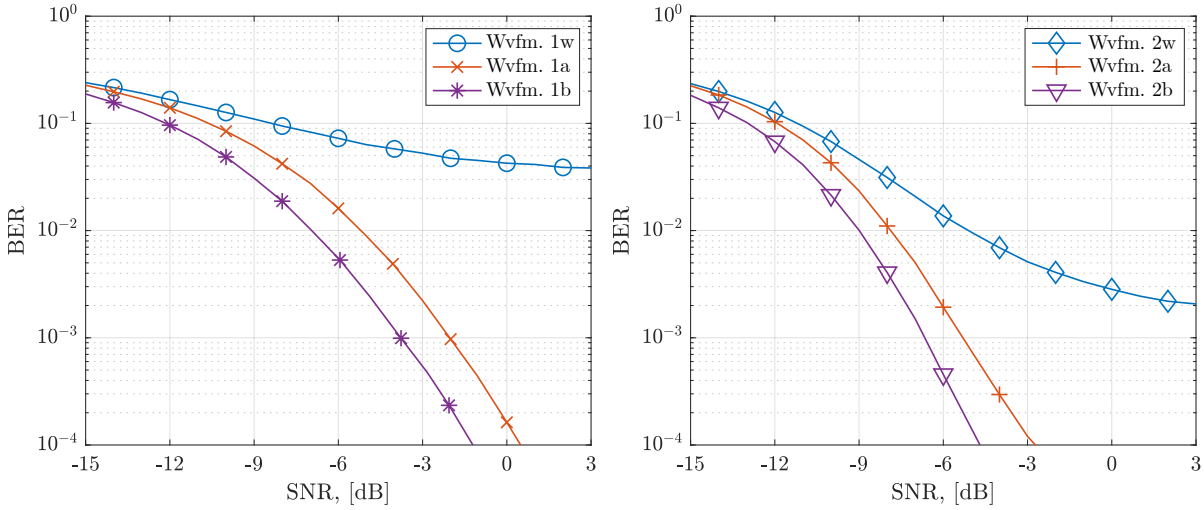

(a) Group 1 waveforms

(b) Group 2 waveforms.

Figure 9: Simulated results of transmitting over a time-invariant 2-mode HF channel in the presence of a strong interferer.

translating to improved BER performances of 1.5-2.5 dB. Moreover, from the 2-mode HF simulation results, it can be seen that both systems effectively combat ISI in the channel. Finally, the results in the presence of a strong narrowband interferer demonstrated the fact that, while the Walsh waveform has severe performance loss, the FBMC-SS system is still able to recover data contained in the un-interfered portion of the transmission band allowing for accurate signal reconstruction at the expense of reduced processing gain proportional to the number of lost subcarriers.

6 Over-the-Air Results

To validate the results generated via simulation, OTA data was collected for the six waveforms listed in Table 1. Data was collected on three different days in each the spring, summer, and fall of 2021 with each test conducted from a different pair of transmitter and receiver locations. All of the collected results were transmitted via skywave and through the same chain of transmit hardware with the exception of the antenna. The transmit packets were interleaved such that the Walsh and FBMC-SS packets were sent alternately in effort to minimize channel differences for both waveforms.

The first of the three links is 300 km between a transmitter in Idaho Falls, ID, and a receiver in Salt Lake City, UT. The carrier frequency was 6.116 MHz and data collection was performed between 3:00pm and 5:00pm in the Mountain Time (MT) zone on May 13$^{\text{th}}$, 2021.

The second set of tests were over an 880 km link between a transmitter in Spokane, WA, and a receiver in Salt Lake City, UT. The transmitter used a constant 8.190 MHz carrier frequency and data collection was performed between 5:30pm and 7:00pm MT on September 15$^{\text{th}}$, 2021.

The final set of tests were over a 4800 km link between Honolulu, HI, and Idaho Falls, ID. A carrier frequency of 15.300 MHz was used, and the data was collected from 4:00pm to 5:00pm MT on November 17$^{\text{th}}$.

For brevity, only the final OTA results are presented here. Other OTA results were similar to the presented results, here.

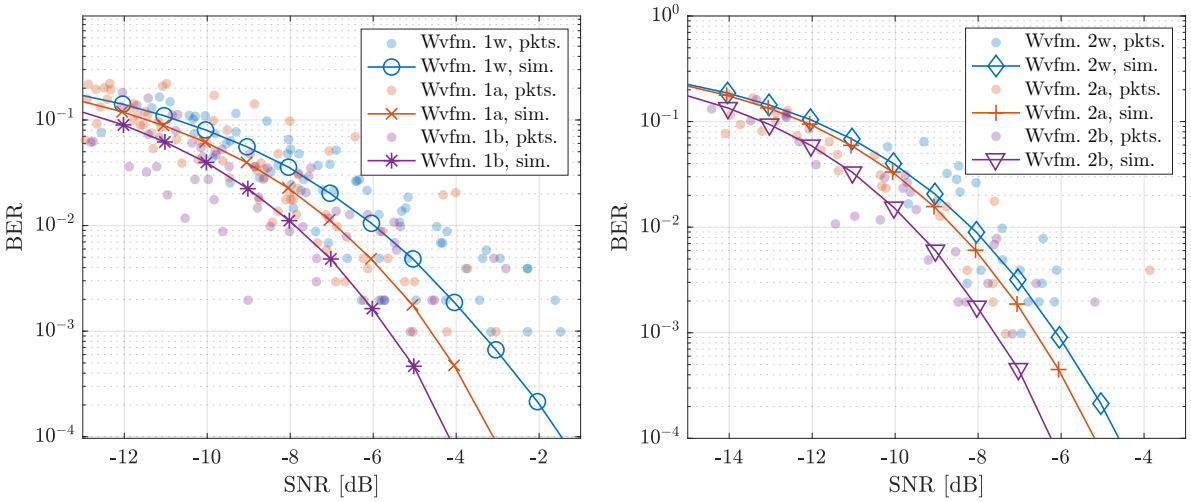

(a) Group 1 waveforms.

(b) Group 2 waveforms.

Figure 10: OTA results between Honolulu, HI and Idaho Falls, ID.

6.1 OTA BER Performance

The channels observed during OTA testing generally matched the channels used in simulation. The delay spread for the three OTA channels ranged from around 90 μs for the shortest to around 1100 μs for the longest delay spreads. The channel observed between Honolulu and Idaho Falls was a 2-mode channel with a mode spacing of around 200 μs. All the channels we observed had Doppler spreads less than 0.2 Hz. The Doppler spreading observed here is substantially less than the Doppler spreads of 2.4 Hz reported in [29], but on the same order as the Doppler spreads reported for quiet conditions in the ITU-R standards [34]. For the long-haul latitudinal link in [35], which is similar to our link between Hawaii and Idaho, the maximum observed Doppler spread was only 0.963 Hz, with a median of 0.245 Hz. Generally, the channels we observed are aligned with the channels reported in [20, 35–38].

By following the definition of coherence time from [9], we find that the OTA channel we observed had a coherence time of around 1.25 seconds, so each transmitted packet observed a relatively time-invariant channel.

Given that the delay and Doppler spreads of the OTA channels are similar to the channels used in simulation, the OTA performance should be similar to that of the simulated results so long as there are no other unexpected detriments present in the channel, such as co-channel interferers. Figs. 10a and 10b show BER vs. SNR results for all 6 waveform types over the link between Honolulu and Idaho Falls. Each individually decoded packet is represented by a point, and each line represents the corresponding 1-mode HF channel simulation result presented previously.

6.2 OTA BER Performance with Interference

The results of the previous section are extended by adding an artificially-generated 3 kHz wide interference. The interference has a flat spectrum over the passband and a constant power-spectral density of 15 dB greater than the signal. Figs. 11a and 11b show the results of this test.

From these figures, it can be seen that the Walsh waveform again approaches an unresolvable bit-error floor at which the SNR no longer influences the BER, mirroring the results obtained via simulation. Conversely, the FBMC-SS systems remain robust against partial band interference.

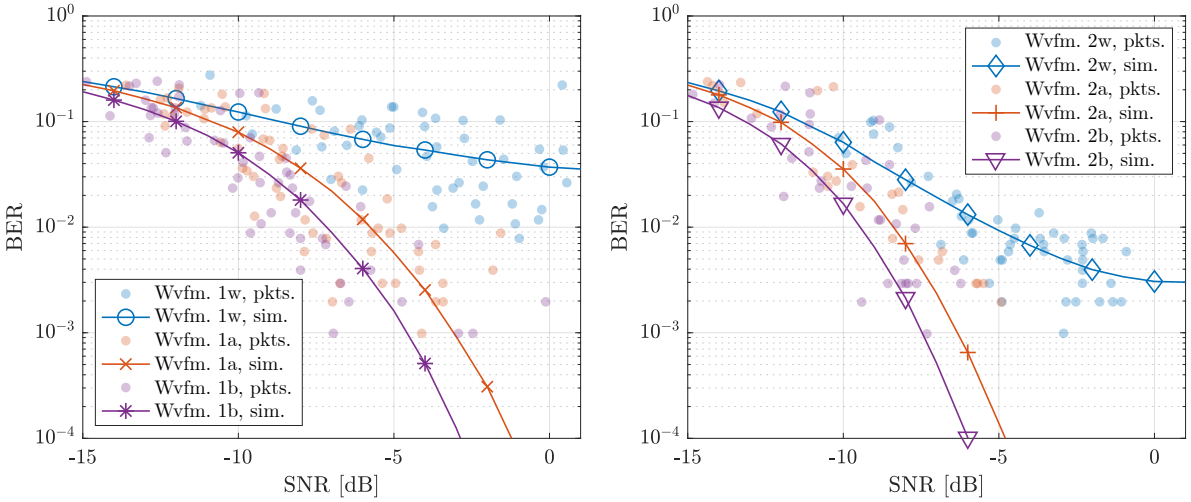

(a) Group 1 waveforms.

(b) Group 2 waveforms.

Figure 11: OTA results between Honolulu, HI and Idaho Falls, ID with the addition of a 3 kHz wide interferer with constanst power spectral density 15 dB greater than the signal power.

7 Conclusion

This paper presented a detailed comparison of the FBMC-SS waveform with waveform 0 of the MIL-STD-188-110D, Appendix D document (namely, Walsh-DSSS waveform), when both are used for communications through the skywave HF channels. Comparisons were done both through computer simulations and by examining test signals that were transmitted over 3 different HF links. All results confirmed the superiority of the FBMC-SS over the Walsh-DSSS waveform. In particular, it was noted that the ability of FBMC-SS to suppress narrowband interferers can greatly benefit communications over skywave HF channels where narrowband interferers are likely to be present. Our findings pose FBMC-SS as a new candidate waveform that may contend as an addition to future HF standards, such as STANAG or MIL-STD documentations.

References

[1] Department of Defense, "MIL-STD-188-110D APPENDIX D,"

[2] J. Wang, G. Ding, and H. Wang, "HF communications: Past, present, and future," *China Communications*, vol. 15, no. 9, pp. 1–9, 2018.

[3] R. M. A. Pages, P. B. Carames, J. C. S. Carrie, and M. D. Herraiz, "Multiresolutive acquisition technique for DS-SS long-haul HF data link," in *The Institution of Engineering and Technology 11th International Conference on Ionospheric radio Systems and Techniques (IRST 2009)*, pp. 1–5, 2009.

[4] E. Johnson, E. Koski, W. Furman, M. Jorgenson, and J. Nieto, *Third-Generation and Wideband HF Radio Communications*. Artech House, 2012.

[5] M. Deumal, C. Vilella, J. Socoro, R. Alsina, and J. Pijoan, "A DS-SS signaling based system proposal for low snr hf digital communications," in *2006 10th IET International Conference on Ionospheric Radio Systems and Techniques (IRST 2006)*, pp. 128–132, 2006.

[6] L. Mattioni and G. Marrocco, "Design of a broadband hf antenna for multimode naval communications," *IEEE Antennas and Wireless Propagation Letters*, vol. 4, pp. 179–182, 2005.

[7] B. Witvliet and R. Alsina-Pagès, "Radio communication via near vertical incidence skywave propagation: an overview," *Telecommunication Systems*, vol. 66, p. 295–309, Feb 2017.

[8] T. Arikan and A. Singer, "Receiver designs for low-latency HF communications," *IEEE Transactions on Wireless Communications*, vol. 20, no. 5, pp. 3005–3015, 2021.

[9] D. Tse and P. Viswanath, *Fundamentals of Wireless Communications*. Cambridge University Press, 1 ed., 2005.

[10] K. Cheun, "Performance of direct-sequence spread-spectrum rake receivers with random spreading sequences," *IEEE Transactions on Communications*, vol. 45, no. 9, pp. 1130–1143, 1997.

[11] P. Bergadà, R. Alsina-Pagès, J. Piljoan, M. Salvador, J. Regué, D. Badia, and S. Graells, "Digital transmission techniques for a long haul HF link: DSSS versus OFDM," *Radio Science*, vol. 49, p. 518–530, Jun 2014.

[12] B. Farhang-Boroujeny and C. Furse, "A robust detector for multicarrier spread spectrum transmission over partially jammed channels," *IEEE Transactions on Signal Processing*, vol. 53, no. 3, pp. 1038–1044, 2005.

[13] D. B. Haab, H. Moradi, T. Holschuh, and B. Farhang-Boroujeny, "Performance analysis of filter bank multicarrier spread spectrum with biorthogonal signaling," in *2020 International Conference on Computing, Networking and Communications (ICNC)*, pp. 902–907, 2020.

[14] S. A. Laraway, H. Moradi, and B. Farhang-Boroujeny, "HF band filter bank multi-carrier spread spectrum," *Proceedings - IEEE Military Communications Conference MILCOM*, vol. 2015-Decem, pp. 1445–1453, 2015.

[15] T. Sibbett, H. Moradi, and B. Farhang-Boroujeny, "Normalized matched filter for blind interference suppression," in *MILCOM 2018 - 2018 IEEE Military Communications Conference (MILCOM)*, pp. 1–6, 2018.

[16] D. L. Wasden, H. Moradi, and B. Farhang-Boroujeny, "Design and implementation of an underlay control channel for cognitive radios," *IEEE Journal on Selected Areas in Communications*, vol. 30, no. 10, pp. 1875–1889, 2012.

[17] D. Haab, H. Moradi, and B. Farhang-Boroujeny, "Spread spectrum symbol detection with blind interference suppression in FBMC-SS," *IEEE Open Journal of the Communications Society*, 2021.

[18] T. Song, W. E. Stark, T. Li, and J. K. Tugnait, "Optimal multiband transmission under hostile jamming," *IEEE Transactions on Communications*, vol. 64, no. 9, pp. 4013–4027, 2016.

[19] R. Folkesson and K.-A. Markström, "Performance limitations in HF communication systems composed of practical realisable hardware," in *The Nordic HF Conference HF19*, pp. 4.1.1–4.1.14, 2019.

[20] S. A. Laraway, J. Loera, H. Moradi, and B. Farhang-Boroujeny, "Experimental comparison of FB-MC-SS and DS-SS in HF channels," in *MILCOM 2018 - 2018 IEEE Military Communications Conference (MILCOM)*, pp. 714–719, 2018.

[21] C.-L. I and R. Gitlin, "Multi-code CDMA wireless personal communications networks," in *Proceedings IEEE International Conference on Communications ICC '95*, vol. 2, pp. 1060–1064 vol.2, 1995.

[22] B. T. Hunt, D. B. Haab, T. C. Sego, T. V. Holschuh, H. Moradi, and B. Farhang-Boroujeny, "Examining the performance of Walsh-DSSS against FBMC-SS in HF channels," in *MILCOM 2021 - 2021 IEEE Military Communications Conference (MILCOM)*, pp. 658–663, 2021.

[23] B. T. Hunt, D. B. Haab, T. C. Sego, T. V. Holschuh, H. Moradi, and B. Farhang-Boroujeny, "Examining the performance of MIL-STD-188-110D waveform 0 against FBMC-SS over skywave HF channels," *[Manuscript submitted for publication]*, 2022.

[24] B. Farhang-Boroujeny, *Adaptive Filters: Theory and Applications*. John Wiley & Sons, Inc., 2 ed., 2013.

[25] Kyungwhoon Cheun, Kwonhue Choi, Hyoungsoo Lim, and Kwangeog Lee, "Antijamming performance of a multicarrier direct-sequence spread-spectrum system," *IEEE Transactions on Communications*, vol. 47, no. 12, pp. 1781–1784, 1999.

[26] G. K. Kaleh, "Frequency-diversity spread-spectrum communication system to counter bandlimited Gaussian interference," *IEEE Transactions on Communications*, vol. 44, pp. 886–893, Jul 1996.

[27] S. Kondo and B. Milstein, "Performance of multicarrier ds cdma systems," *IEEE Transactions on Communications*, vol. 44, no. 2, pp. 238–246, 1996.

[28] M. Friese, "Multitone signals with low crest factor," *IEEE Transactions on Communications*, vol. 45, pp. 1338–1344, Oct 1997.

[29] J. Mastrangelo, J. Lemmon, L. Vogler, J. Hoffmeyer, L. Pratt, and C. Behm, "A new wideband high frequency channel simulation system," *IEEE Transactions on Communications*, vol. 45, no. 1, pp. 26–34, 1997.

[30] C. Watterson, J. Juroshek, and W. Bensema, "Experimental confirmation of an HF channel model," *IEEE Transactions on Communication Technology*, vol. 18, no. 6, pp. 792–803, 1970.

[31] T. Wang, J. G. Proakis, and J. R. Zeidler, "Interference analysis of filtered multitone modulation over time-varying frequency- selective fading channels," *IEEE Transactions on Communications*, vol. 55, no. 4, pp. 717–727, 2007.

[32] J.-Z. Fu, L.-L. Guo, H.-Q. Yang, and Z.-X. Han, "Narrow-band interference suppression in DSSS systems using efficient adaptive filters," in *2009 WRI International Conference on Communications and Mobile Computing*, vol. 1, pp. 353–357, 2009.

[33] A. Syed and A. Rizvi, "Narrowband interference suppression techniques in direct sequence spread spectrum communication system," in *Proceedings. IEEE International Multi Topic Conference, 2001. IEEE INMIC 2001. Technology for the 21st Century.*, pp. 178–184, 2001.

[34] ITU-R Recommendation F.1487, "Testing of HF modems with bandwidths of up to about 12 kHz using ionospheric channel simulators," 2000.

[35] M. Clune, P. Fine, J. Freedman, C. Nissen, and B. Perry, "Delay and doppler spreading characteristics of the wide-bandwidth HF channel," in *1991 Fifth International Conference on HF Radio Systems and Techniques*, pp. 194–198, 1991.

[36] M. Tooby, P. Arthur, P. Cotterill, N. Hoult, and J. Whiffen, "An assessment of the propagation characteristics of the hf nvis channel," in *2000 Eighth International Conference on HF Radio Systems and Techniques*, pp. 263–267, 2000.

[37] A. Jain, P. Pagani, R. Fleury, M. M. Ney, and P. Pajusco, "Cross-channel sounding for HF geolocation: Concepts and experimental results," in *12th European Conference on Antennas and Propagation (EuCAP 2018)*, pp. 1–5, 2018.

[38] W. Furman and J. Nieto, "Understanding HF channel characteristics via spectrogram interpretation and modelling," pp. 1.1.1–1.1.12, 2016.